Dalton Transactions

PAPER

View Article Online
View Journal | View Issue

Cite this: *Dalton Trans.*, 2017, **46**, 13943

Metal–organic frameworks with 1,4-di(1*H*-imidazol-4-yl)benzene and varied carboxylate ligands for selectively sensing Fe(III) ions and ketone molecules†

Zhi-Qiang Liu,[a] Yue Zhao,[a] Xiu-Du Zhang,[a] Yan-Shang Kang,[a] Qing-Yi Lu,[a] Mohammad Azam,[b] Saud I Al-Resayes[b] and Wei-Yin Sun *[a]

Received 11th August 2017,
Accepted 16th September 2017

DOI: 10.1039/c7dt02981k

rsc.li/dalton

Four new metal–organic frameworks (MOFs) $[Zn(L)(bpdc)]\cdot 1.6H_2O$ (**1**), $[Co(L)(bpdc)]\cdot H_2O$ (**2**), $[Ni_3(L)_2(bptc)_2(H_2O)_{10}]\cdot 2H_2O$ (**3**) and $[Cd_2(L)(Hbptc)_2]$ (**4**) were achieved by reactions of the corresponding metal salt with mixed organic ligands of 1,4-di(1*H*-imidazol-4-yl)benzene (L) and 4,4′-benzophenonedicarboxylic acid (H_2bpdc) or biphenyl-2,4′,5-tricarboxylic acid (H_3bptc). They exhibit varied structures: MOFs **1** and **4** are porous three-dimensional (3D) frameworks, while **2** is an infinite one-dimensional (1D) chain and **3** is a two-dimensional (2D) network. Remarkably, **1** and **4** can act as potential fluorescent materials for sensing Fe(III) ions and different ketone molecules with high selectivity and sensitivity. In addition, MOF **1** shows selective adsorption of CO_2 over N_2.

Introduction

Metal–organic frameworks (MOFs), as a new class of inorganic–organic hybrid materials, have received extensive attention for their structural diversity, interesting properties as well as potential application in fields such as gas storage/separation, luminescence, catalysis and chemical sensing.[1–10] Particularly, fluorescence sensing based on luminescent MOFs has been developed rapidly due to its advantage of short response time, low cost, high sensitivity and efficiency,[11,12] and varied MOF-based fluorescent sensors have been established in recent years. Luminescent MOFs have been utilized to probe small organic molecules and metal ions *via* fluorescence enhancing or quenching.[13–17] However, it is still a challenge to rationally design and synthesize MOFs with definite structures and desired properties because there are factors including reaction temperature and solvent, auxiliary ligand and metal center affecting the framework structure and property of the resulting MOFs.

On the other hand, organic ligands are critical in the construction of MOFs. Our previous studies have demonstrated that organic compounds with 1*H*-imidazol-4-yl groups are versatile ligands for the construction of MOFs with definite structures and properties. Such 1*H*-imidazol-4-yl groups can act as both anionic and neutral ligands with and without deprotonation of the NH group.[18,19] Moreover, carboxylate ligands provide abundant coordination modes. On the basis of the advantage of the nitrogen donor and carboxylate ligands, the strategy using mixed carboxylate and nitrogen donor ligands is powerful in the construction of MOFs. In this work, four new MOFs have been successfully synthesized *via* the utilization of 1,4-di(1*H*-imidazol-4-yl)benzene (L) and different multi-carboxylate ligands with transition metal salts. Namely, $[Zn(L)(bpdc)]\cdot 1.6H_2O$ (**1**), $[Co(L)(bpdc)]\cdot H_2O$ (**2**), $[Ni_3(L)_2(bptc)_2(H_2O)_{10}]\cdot 2H_2O$ (**3**) and $[Cd_2(L)(Hbptc)_2]$ (**4**) (H_2bpdc = 4,4′-benzophenonedicaboxylic acid, H_3bptc = biphenyl-2,4′,5-tricarboxylic acid) have been achieved. They were characterized by X-ray crystallography, thermal and elemental analyses. Adsorption, photoluminescence and sensing properties of the complexes were investigated.

Experimental

Materials and methods

All commercially available chemicals and solvents are of reagent grade and were used as received without further purification. Ligand L was prepared according to the

[a]*Coordination Chemistry Institute, State Key Laboratory of Coordination Chemistry, School of Chemistry and Chemical Engineering, Nanjing National Laboratory of Microstructures, Collaborative Innovation Center of Advanced Microstructures, Nanjing University, Nanjing 210023, China. E-mail: sunwy@nju.edu.cn; Tel: +86 25 89683485*

[b]*Department of Chemistry, College of Science, King Saud University, P. O. Box 2455, Riyadh 11451, Kingdom of Saudi Arabia*

†Electronic supplementary information (ESI) available: PXRD, TG and additional figures. CCDC 1549985–1549988. For ESI and crystallographic data in CIF or other electronic format see DOI: 10.1039/c7dt02981k

reported procedures.[20] FT-IR spectra were recorded in the range of 4000–400 cm^{-1} on a Bruker Vector 22 FT-IR spectrometer using KBr pellets. Powder X-ray diffraction (PXRD) measurements were performed on a Bruker D8 Advance. Elemental analyses (EA) for C, H, and N were carried out on a PerkinElmer 240C elemental analyzer. Thermogravimetric analyses (TGA) were taken on a Mettler-Toledo (TGA/DSC1) thermal analyzer at a heating rate of 10 °C min^{-1} under the nitrogen atmosphere. Photoluminescence spectra were obtained on an Aminco Bowman Series 2 spectrofluorometer with a xenon arc lamp as the light source. In the measurements of emission and excitation spectra, the pass width is 5 nm. Gas sorption data were collected on a Belsorp-max volumetric gas sorption instrument.

Synthesis of $[Zn(L)(bpdc)]\cdot 1.6H_2O$ (1). A mixture of L (21.0 mg, 0.10 mmol), $Zn(NO_3)_2\cdot 6H_2O$ (29.8 mg, 0.10 mmol) and H_2bpdc (27.0 mg, 0.10 mmol) in DMF/H_2O (1 : 3) (10 ml) was sealed in a Teflon-lined stainless steel container and heated at 120 °C for 3 days. After being cooled to room temperature, colorless crystals of **1** were obtained in 65% yield. Anal. calcd for $C_{27}H_{21.2}N_4O_{6.6}Zn$: C, 56.63; H, 3.73; N, 9.78%. Found: C, 56.44; H, 3.82; N, 9.66%. IR (KBr pellet, cm^{-1}, Fig. S11†): 3450 (w), 3131(w), 1655(m), 1595(s), 1545(s), 1502(m), 1412(s), 1269(s), 1135(w), 931(w), 847(m), 730(s), 650(m), 533(w).

Synthesis of $[Co(L)(bpdc)]\cdot H_2O$ (2). A mixture of L (21.0 mg, 0.10 mmol), $Co(NO_3)_2\cdot 6H_2O$ (29.8 mg, 0.10 mmol), H_2bpdc (27.0 mg, 0.10 mmol) and NaOH (8.0 mg, 0.2 mmol) in H_2O (10 ml) was sealed in a Teflon-lined stainless steel container and heated at 120 °C for 3 days. After being cooled to room temperature, block crystals of **2** were obtained in 65% yield. Anal. calcd for $C_{27}H_{20}N_4O_6Co$: C, 58.39; H, 3.63; N, 10.09%. Found: C, 58.32; H, 3.72; N, 10.02%. IR (KBr pellet, cm^{-1}, Fig. S11†): 3500(w), 3130(m), 1663(m), 1590(s), 1533(s), 1507(m), 1423(s), 1270(m), 1128(w), 855(m), 730(m), 651(m), 527(w).

Synthesis of $[Ni_3(L)_2(bptc)_2(H_2O)_{10}]\cdot 2H_2O$ (3). A mixture of L (21.0 mg, 0.10 mmol), $Ni(NO_3)_2\cdot 6H_2O$ (29.1 mg, 0.10 mmol), H_3bptc (19.1 mg, 0.067 mmol) and NaOH (8.0 mg, 0.2 mmol) in H_2O (10 ml) was sealed in a Teflon-lined stainless steel container and heated at 120 °C for 3 days. After being cooled to room temperature, green block crystals of **3** were obtained in 75% yield. Anal. calcd for $C_{54}H_{58}N_8O_{24}Ni_3$: C, 47.03; H, 4.24; N, 8.12%. Found: C, 46.93; H, 4.42; N, 8.16%. IR (KBr pellet, cm^{-1}, Fig. S11†): 3602(m), 3257(m), 1557(s), 1394(s), 1373(s), 1139(m), 811(m), 640(w), 525(w).

Synthesis of $[Cd_2(L)(Hbptc)_2]$ (4). Complex **4** was obtained by the same procedure used for the preparation of **3** except that the metal salt was replaced by $Cd(NO_3)_2\cdot 4H_2O$ (30.8 mg, 0.10 mmol). Colorless crystals of **4** were obtained in 71% yield. Anal. calcd for $C_{42}H_{26}N_4O_{12}Cd_2$: C, 50.27; H, 2.61; N, 5.58%. Found: C, 50.13; H, 2.72; N, 5.56%. IR (KBr pellet, cm^{-1}, Fig. S11†): 3450(w), 3167(m), 1669 (s), 1607(s), 1584(s), 1552(s), 1399(s), 1349(s), 1282(m), 1258(m), 1139(m), 948(w), 818(m), 760(m), 708(w), 645(w), 515(w).

X-ray crystallography

Crystallographic data for **1–4** were collected on a Bruker Smart Apex II CCD area-detector diffractometer with graphite-monochromated Mo Kα radiation (λ = 0.71073 Å). The integration of the diffraction data as well as the intensity corrections for the Lorentz and polarization effects was carried out using the SAINT program.[21] Semi-empirical absorption correction was performed using SADABS program.[22] The structures of **1–4** were solved by direct methods using SHELXS-2014 and all the non-hydrogen atoms were refined anisotropically on F^2 by the full-matrix least-squares technique with SHELXL-2014.[23,24] The hydrogen atoms except for those of water molecules were generated geometrically and refined isotropically using the riding model. Because the free solvent molecules in **1** are highly disordered and impossible to refine using conventional discrete-atom models, the SQUEEZE subroutine of the PLATON software suite was used to remove the scattering from the highly disordered solvent molecules.[25,26] The formula of **1** was obtained based on volume/count_electron analysis, TG and elemental analyses. The reported refinements are of the guest-free structures obtained by the SQUEEZE routine, and the results are attached to the CIF file. The details of the crystal parameters, data collection and refinements for the complexes are summarized in Table 1 and selected bond lengths and angles are listed in Table S1.† The hydrogen bonding data are provided in Table S2.†

Results and discussion

Crystal structure description

Crystal structure of $[Zn(L)(bpdc)]\cdot 1.6H_2O$ (1). The results of structural analysis revealed that **1** crystallizes in the orthorhombic *Pnna* space group. The asymmetric unit of **1** consists of one Zn(II), one $bpdc^{2-}$ and one L (Fig. 1a). Zn1 is six-coordinated with distorted octahedral coordination geometry by two nitrogen atoms (N1, N1B) from two different L and four oxygen ones (O1, O2, O1B, O2B) from two different $bpdc^{2-}$. The Zn–O bond distances are 2.048(3) and 2.444(3) Å, while the Zn–N one is 2.006(3) Å. The coordination angles around Zn(II) is from 57.91(10) to 152.86(12)° (Table S1†). Each L links two Zn(II) atoms to form an infinite one-dimensional (1D) zigzag chain (Fig. S1†), and each $bpdc^{2-}$ connects two Zn(II) atoms using its two carboxylate groups each with a μ_1–η^1:η^1-chelating mode (Scheme S1a†) to give an infinite 1D zigzag chain (Fig. S1†). Then, two kinds of 1D chains cross-link together to give a three dimensional (3D) framework of **1** (Fig. 1b). Due to the presence of large vacancy, it is apt to form an interpenetrating framework, accordingly, the final structure of **1** is a 3-fold interpenetrating framework as illustrated in Fig. 1c. The solvent accessible volume for **1** calculated by PLATON is 604.0 $Å^3$ per 2787.4 $Å^3$ unit cell volume (21.7% of the crystal volume).

To simplify the 3D structure of **1**, topological analysis was performed. As shown in Fig. 1c, Zn(II), L and $bpdc^{2-}$ can be regarded as four-, two-, and two-connectors, respectively.

Table 1 Crystal data and structure refinements for 1–4

Compound	1	2	3	4
Formula	$C_{27}H_{21.2}N_4O_{6.6}Zn$	$C_{27}H_{20}N_4O_6Co$	$C_{54}H_{58}N_8O_{24}Ni_3$	$C_{21}H_{13}N_2O_6Cd$
Formula weight	572.69	555.40	1379.21	501.73
Crystal system	Orthorhombic	Monoclinic	Triclinic	Triclinic
Space group	*Pnna*	$P2_1/c$	$P\bar{1}$	$P\bar{1}$
a (Å)	11.0779(11)	11.4041(9)	7.096(5)	9.2381(7)
b (Å)	22.030(2)	21.3552(16)	13.946(5)	10.1167(8)
c (Å)	11.4217(10)	10.8848(8)	15.121(5)	11.7020(8)
α (°)	90	90	78.028(5)	82.635(2)
β (°)	90	99.7010(10)	79.552(5)	71.861(2)
γ (°)	90	90	88.318(5)	63.266(2)
V (Å^3)	2787.4(4)	2612.9(3)	1439.5(12)	928.12(12)
Z	4	4	1	2
D_c (g cm^{-3})	1.296	1.412	1.591	1.795
μ (mm^{-1})	0.922	0.705	1.063	1.220
F (000)	1112	1140	714	498
Data collected	15 068	17 672	12 793	3982
Unique reflections	3211	6012	6592	2873
Goodness-of-fit	0.920	1.028	1.056	1.064
R_1 [a] $[I > 2\sigma(I)]$	0.0655	0.0361	0.0435	0.0474
wR_2 [b] $[I > 2\sigma(I)]$	0.1655	0.0932	0.0996	0.1303

[a] $R_1 = \sum||F_o| - |F_c||/\sum|F_o|$. [b] $wR_2 = |\sum w(|F_o|^2 - |F_c|^2)|/\sum|w(F_o)^2|^{1/2}$, where $w = 1/[\sigma^2(F_o^2) + (aP)^2 + bP]$. $P = (F_o^2 + 2F_c^2)/3$.

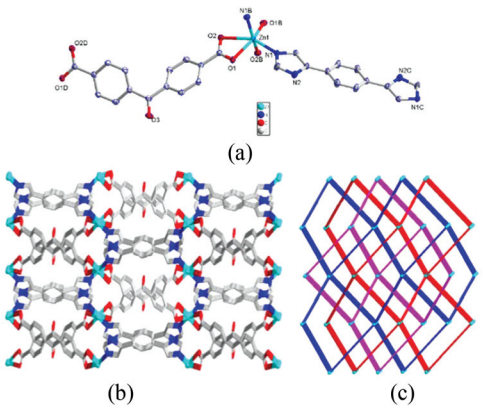

Fig. 1 (a) Coordination environment of Zn(II) in 1 with ellipsoids drawn at 30% probability level. Hydrogen atoms and free solvent molecules are omitted for clarity. (b) 3D structure of 1. (c) Topology and 3-fold interpenetration of 1.

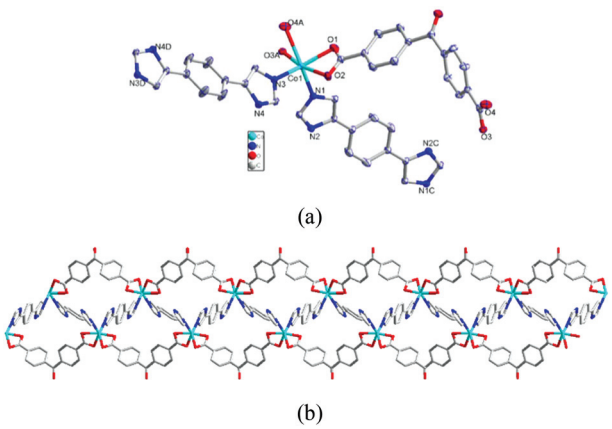

Fig. 2 (a) Coordination environment of Co(II) in 2 with the ellipsoids drawn at the 30% probability level. Hydrogen atoms and free water molecules are omitted for clarity. (b) 1D chain structure of 2.

Therefore, the resulting structure of **1** is a 4-connected dmp net with a Schläfli symbol of $(6^5{\cdot}8)$ topology calculated by TOPOS program.[27,28]

Crystal structure of [Co(L)(bpdc)]·H$_2$O (2). When $Co(NO_3)_2{\cdot}6H_2O$ instead of $Zn(NO_3)_2{\cdot}6H_2O$ was used in the reaction, **2** was obtained. The results of single crystal X-ray diffraction analysis indicate that **2** crystallizes in monoclinic space group $P2_1/c$. As depicted in Fig. 2a, Co1 has a N_2O_4 donor set with four carboxylate oxygen atoms (O1, O2, O3A, O4A) from two different $bpdc^{2-}$ and two imidazole nitrogen ones (N1, N3) from two distinct L ligands. The Co–N bond distances are 2.0389(15) and 2.0633(15) Å, and the Co–O ones are in the range of 2.0784(14)–2.3513(16) Å. The bond angles around Co(II) are from 58.51(5) to 169.10(5)° (Table S1†). Each L links two Co(II) atoms to form an infinite zigzag 1D chain (Fig. S2†), and each $bpdc^{2-}$ connects two Co(II) atoms using its two carboxylate groups each with a μ_1–η^1:η^1-chelating mode (Scheme S1a†) to form an infinite linear 1D chain (Fig. S2†). It is clear that the coordination of metal centers and linkage modes of L and $bpdc^{2-}$ ligands are almost the same for **1** and **2**; however, two kinds of 1D chains cross-link together to generate an infinite 1D chain of **2** (Fig. 2b), rather than the 3D framework of **1** (Fig. 1b). The 1D chain of **2** is further joined together through hydrogen bonding interactions to give the eventual 3D supramolecular structure of **2** (Fig. S3 and Table S2†).

Crystal structure of [Ni$_3$(L)$_2$(bptc)$_2$(H$_2$O)$_{10}$]·2H$_2$O (3). To further investigate the effect of the carboxylate ligand on the structure of the complex, H_3bptc, instead of the H_2bpdc, was used in the reaction and **3** with a different structure was successfully isolated. Single crystal X-ray diffraction analysis con-

firmed that **3** crystallizes in the triclinic crystal system and space group $P\bar{1}$. The asymmetric unit of **3** is a half molecule of $[Ni_3(L)_2(bptc)_2(H_2O)_{10}]\cdot 2H_2O$ and includes two Ni(II) atoms, one of which is sitting on an inversion center. As exhibited in Fig. 3a, Ni1 atom is six-coordinated with octahedral coordination geometry and surrounded by two nitrogen atoms (N3, N3C) from two different L, two carboxylate oxygen ones (O3, O3C) from two $bptc^{3-}$ and two coordinated water molecules (O10, O10C). The Ni–N bond length is 2.044(2) Å and that of the Ni1–O ones are 2.0644(17) Å and 2.122(2) Å. In addition, the coordination angles around Ni1 span from 87.97(8) to 180.0° (Table S1†). While Ni2 is surrounded by one carboxylate oxygen atom (O1) from $bptc^{3-}$, one imidazole nitrogen (N1) from L and four coordinated water molecules (O7, O8, O9, O12). The Ni2–N bond length is 2.045(2) Å, while the Ni2–O ones are in the range of 2.032(2)–2.114(2) Å. The coordination angles around Ni2 are from 85.24(9) to 178.05(8)° (Table S2†). L ligands link Ni(II) atoms to form an infinite 1D chain (Fig. S4†), and $bptc^{3-}$ adopts a μ_2-bridging mode to connect two Ni(II) atoms using its two carboxylate groups with the $(\mu_1\text{–}\eta^1\text{:}\eta^0)$-$(\mu_1\text{–}\eta^1\text{:}\eta^0)$-bptc coordination mode (Scheme S1b†). The Ni(II)-L 1D chains are further connected by $bptc^{3-}$ ligands to generate a 2D network structure of **3** (Fig. 3b), which is further extended into a 3D supramolecular architecture through O–H···O hydrogen bonds (Fig. S5 and Table S2†).

Crystal structure of $[Cd_2(L)(Hbptc)_2]$ (4). When we brought in another kind of d^{10} metal center of Cd(II) and a new complex **4** was obtained. **4** crystallizes in the triclinic $P\bar{1}$ space group. In the asymmetric unit of **4**, there are one Cd(II), half L and one $Hbptc^{2-}$. As shown in Fig. 4a, Cd1 is five-coordinated

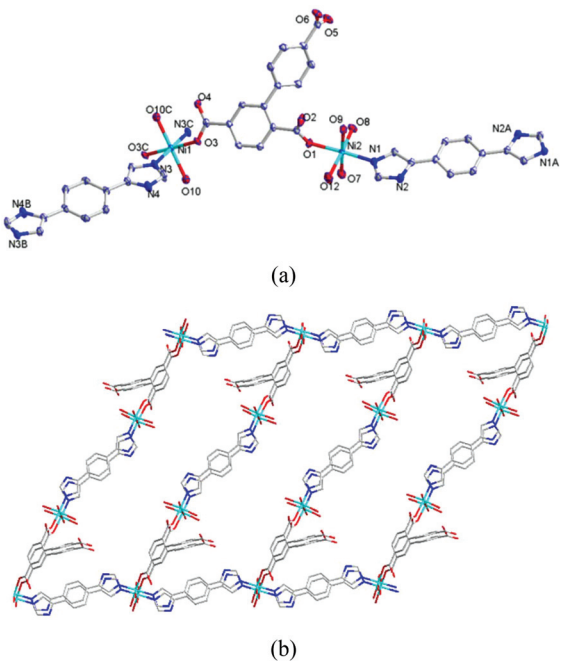

Fig. 3 (a) Coordination environment of Ni(II) in **3** with the ellipsoids drawn at the 30% probability level. Hydrogen atoms and free water molecules are omitted for clarity. (b) 2D structure of **3**.

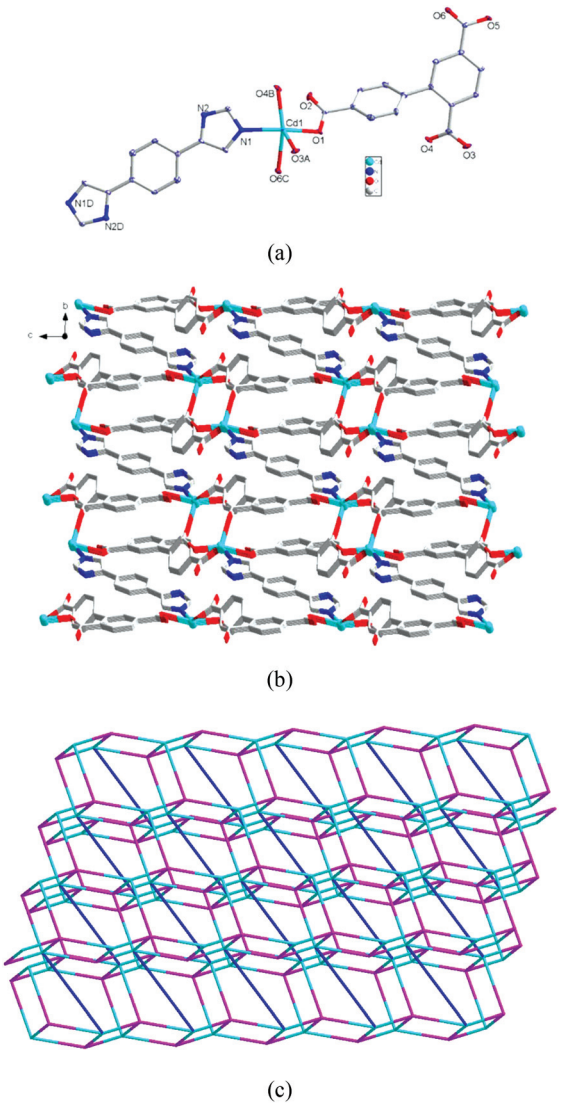

Fig. 4 (a) Coordination environment of Cd(II) in **4** with the ellipsoids drawn at the 30% probability level. Hydrogen atoms are omitted for clarity. (b) 3D framework of **4**. (c) Topology of **4**.

by one nitrogen (N1) from one L and four carboxylate oxygen atoms (O1, O3A, O4B, O6C) form four different $Hbptc^{2-}$ ligands. It is noteworthy that three carboxylate groups of $Hbptc^{2-}$ in **4** exhibit two kinds of coordination modes which are different from those in **3**, each $Hbptc^{2-}$ ligand in **4** connects four metal atoms using its three carboxylate groups with the $(\mu_1\text{–}\eta^1\text{:}\eta^0)$-$(\mu_1\text{–}\eta^1\text{:}\eta^0)$-$(\mu_1\text{–}\eta^1\text{:}\eta^1)$-bptc coordination mode (Scheme S1c†). The $Hbptc^{2-}$ ligands connect Cd(II) atoms to form a 2D network (Fig. S6†). Then the adjacent layers are further connected by L ligands, thereby resulting in the final 3D framework of **4** (Fig. 4b).

Topological analysis was carried out to get insights into the structure of **4**, each 2-connected bridging L ligand can be regarded as a linear linker. Each Cd(II) atom can be regarded as a 5-connected node since it links one L and four $Hbptc^{2-}$ ligands. Each $Hbptc^{2-}$ ligand connects four Cd(II) atoms and

can be treated as a 4-connector. Therefore, the resulting structure of **4** can be simplified as a (4, 5)-connected binodal 3D net, as shown in Fig. 4c. The point (Schläfli) symbol for the net is $\{4^3{\cdot}6^3\}\{4^3{\cdot}6^6{\cdot}8\}$ calculated by TOPOS program.

Comparison of the structures 1–4

The results of crystallographic analyses revealed that MOFs **1–4** show varied structures from the 1D chain (**2**), 2D network (**3**) to 3D frameworks (**1** and **4**). The different structures of **1** and **2** as well as **3** and **4** are attributed to the different metal centers. In addition, the carboxylate ligands exhibit varied coordination modes, in particular, $bptc^{3-}$ in **3** binds two metal atoms while the $Hbptc^{2-}$ in **4** connects four metal centers. The results herein further confirm that the metal center and varied coordination modes of the carboxylate ligand exert subtle but crucial influence on the structural diversity of the frameworks.

Thermogravimetric analysis (TGA) and powder X-ray diffraction (PXRD)

Thermogravimetric analyses (TGA) were performed to check the thermal stability of the frameworks, and the results are shown in Fig. S7.† For **1**, a weight loss of 5.51% was observed in the temperature range of 30–100 °C, which corresponds to the loss of water molecules (calcd 5.03%) and a further weight loss was observed at about 240 °C, corresponding to the collapse of the framework. In the case of **2**, a weight loss was found before 180 °C due to the release of water molecules with a weight loss of 3.11% (calcd 3.24%), and the residue is stable up to 380 °C. The TG curve of **3** shows a weight loss of 16.05% from 30 to 160 °C, corresponding to the loss of free water molecules (calcd 15.66%), and the residue is stable up to about 360 °C. **4** did not show obvious weight losses before the decomposition of the framework at about 380 °C, which is in agreement with the result of the crystal structure. The phase purity of bulk products was confirmed by PXRD measurements, and each PXRD pattern of the as-synthesized sample is consistent with the simulated one (Fig. S8†), implying the pure phases of **1–4**.

Adsorption properties of 1

The structural analysis revealed that there are voids occupied by solvent molecules in **1**. To evaluate the porosity of **1**, adsorption isotherms of N_2 at 77 K and CO_2 at 195 K were measured. The activated sample was prepared by heating the as-synthesized **1** under vacuum at 100 °C for 10 h, and it was found that the free guest molecules in **1** were removed (Fig. S9†) without destroying the framework (Fig. S8a†). As shown in Fig. 5, the sorption curve of N_2 at 77 K for **1** suggests only surface adsorption; however, **1** exhibits typical type-I gas uptake isotherms with a CO_2 adsorption ability of 44.39 $cm^3\ g^{-1}$, corresponding to 1.08 CO_2 molecules per formula unit at 195 K and 1 atm. The results indicate that **1** might be promising materials for selective adsorptive separation of CO_2 from industrial flue gas or the removal of CO_2 from natural gas.

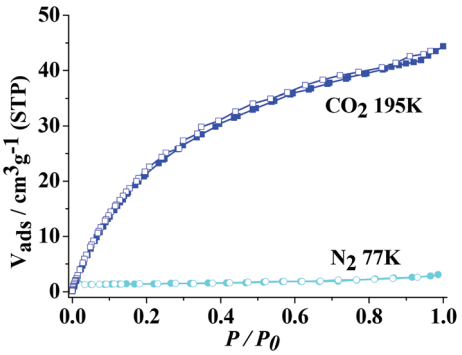

Fig. 5 N_2 (77 K) and CO_2 (195 K) adsorption isotherms of **1** (filled shape, adsorption; open shape, desorption).

Photoluminescence studies

Inorganic–organic hybrid frameworks, especially those with d^{10} metal centers, have potential for fluorescence owing to their ability to adjust the emission of the hybrids.[29] Accordingly, solid-state luminescence emission spectra of **1** and **4** as well as L under the same experimental conditions were measured and the results are exhibited in Fig. S10.† Intense emission was observed at 455 nm for L upon excitation at 340 nm, and emission bands were observed at 580 nm (λ_{ex} = 290 nm) for **1**, 600 nm (λ_{ex} = 300 nm) for **4**. Compared with the free L ligand, the red-shifts of the emissions of **1** and **4** are considered to be caused by the coordination of the ligand to the metal centers.

Sensing small organic molecules

To further explore the potential of luminescent **1** and **4** for sensing small organic molecules, the fluorescence behavior of **1** and **4** immersing in different solvents was investigated. The results clearly show that the emission intensities of **1** and **4** depend on the solvent (Fig. 6); however, only the presence of acetone can quench the fluorescence of **1** and **4** efficiently. The observed fluorescence quenching may be ascribed to the interactions between the framework and acetone molecules, in particular, probably the "C═O" of acetone and the frameworks of **1** and **4**, since such ligand based fluorescence can be quenched by energy transfer between the organic ligands and the acetone molecules.[30–32]

The quenching effect of acetone has been further investigated for **1** and **4** dispersed in DMF suspension. As exhibited in Fig. 7, the luminescence intensity of the suspension significantly decreased with the addition of acetone, and almost disappeared when the acetone amount reached 37 μL for **1** and 30 μL for **4**. The fluorescence decrease was nearly proportional to the acetone concentration and the fluorescence intensity *vs.* the volume ratio of acetone could be fit by a first-order exponential decay (Fig. 8), implying that the fluorescence quenching of **1** and **4** with acetone is diffusion controlled. To examine the luminescence quenching degree, the quantified value of the quenching effect of acetone was obtained using the Stern–Volmer equation: $I_0/I = 1 + K_{SV}[M]$,[33] in which [M] is the molar

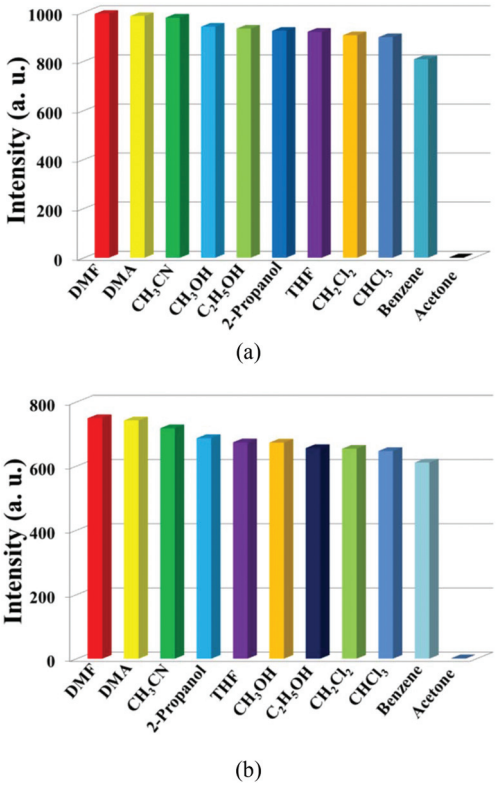

Fig. 6 (a) Photoluminescence intensities of **1** introduced into varied pure solvents when excited at 290 nm for **1**. (b) Photoluminescence intensities of **4** introduced into varied pure solvents when excited at 300 nm for **4**.

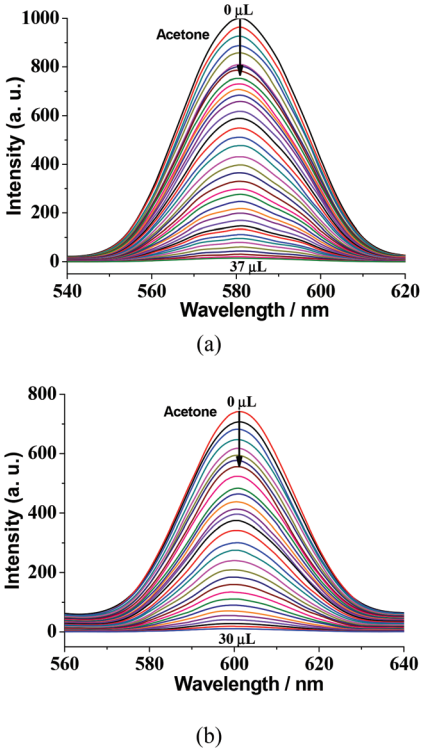

Fig. 7 (a) Photoluminescence spectra of the dispersed **1** in DMF in the presence of varied contents of the acetone (excited at 290 nm). (b) Photoluminescence spectra of the dispersed **4** in DMF in the presence of varied contents of the acetone (excited at 300 nm).

concentration of the analyte, I_0 and I are the luminescence intensities of **1** and **4** dispersed in DMF suspension without and with the addition of acetone, respectively. As shown in Fig. 9, a good linear Stern–Volmer relationship was observed for **1** and **4**, implying that they are the dynamic quenching process for the detection of acetone, the K_{SV} values are calculated to be 0.4788 for **1** and 0.4918 for **4**. By ratio of $3\sigma/S$ (σ is the standard deviation for 10 replicating fluorescence measurements of blank solutions, and S is the slope of the calibration curve), the detection limits for **1** and **4** are estimated to be 0.0478 vol% and 0.0465 vol%, respectively. The results demonstrate that **1** and **4** can selectively sense acetone molecules and have comparably minimal detection amount of acetone with the previously reported MOF-based acetone sensors.[34–36] Thus, **1** and **4** can be considered as a potential candidate for selective sensing of acetone molecules.

In order to explore whether the interaction between the "C═O" of acetone and the frameworks of **1** and **4** causing fluorescence quenching, the fluorescence behavior of **1** and **4** immersing in different ketone molecules was examined. As shown in Fig. 10, among the chosen ketones, stable suspensions of **1** and **4** in cyclohexanone, 4-heptanone and 5-nonanone showed the highest quenching. The results suggest that the fluorescence quenching may be caused by the interaction between "C═O" of ketone and the frameworks of **1** and **4**.

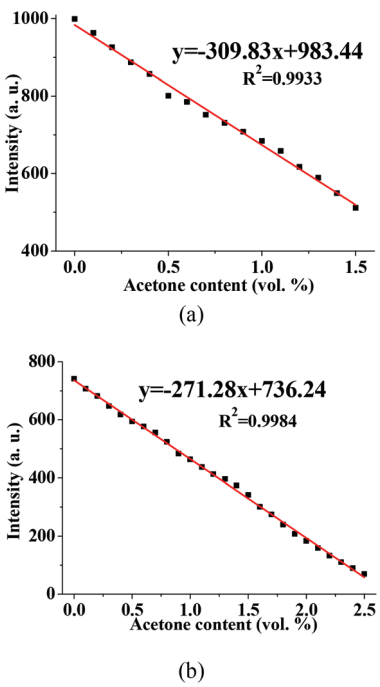

Fig. 8 (a) Photoluminescence intensities of **1** in DMF as a function of acetone content (excited at 290 nm). (b) Photoluminescence intensities of **4** in DMF as a function of acetone content (excited at 300 nm).

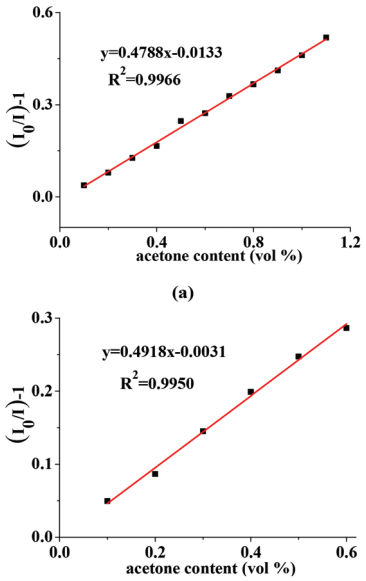

Fig. 9 (a) Stern–Volmer plot of **1** for acetone. (b) Stern–Volmer plot of **4** for acetone.

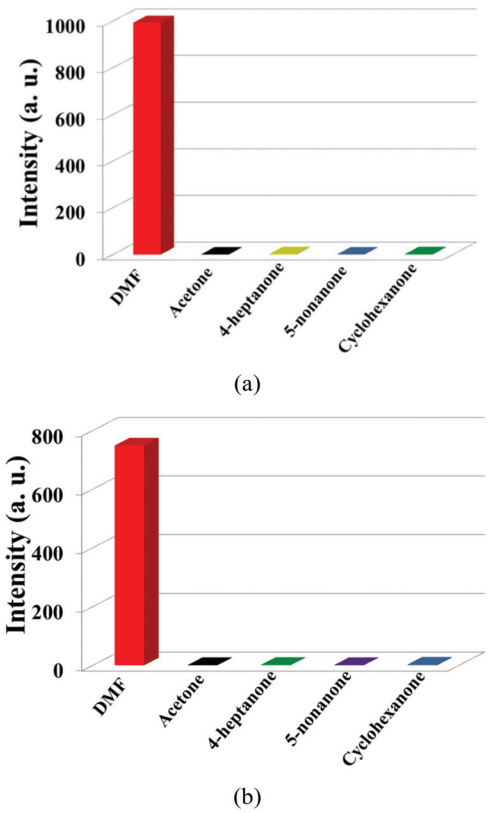

Fig. 10 (a) Photoluminescence intensities of **1** introduced into varied ketone molecules when excited at 290 nm for **1**. (b) Photoluminescence intensities of **4** introduced into varied ketone molecules when excited at 300 nm for **4**.

Thus, **1** and **4** can be considered as a potential candidate for selective sensing of ketone molecules.

Luminescence sensing of Fe(III) ions

The selective recognition ability of **1** and **4** toward metal ions was also investigated. The as-synthesized sample of **1** or **4** (2 mg) was ground and dispersed into DMF solutions containing different $M(NO_3)_x$ with a concentration of [M] = 10^{-3} mol L^{-1} (M = K^+, Li^+, Na^+, Ni^{2+}, Co^{2+}, Pb^{2+}, Zn^{2+}, Cu^{2+}, Cd^{2+}, Mg^{2+}, Al^{3+}, $Cr^{3+}$and Fe^{3+}). Obviously, as shown in Fig. 11, the fluorescence responses of **1** and **4** are strongly dependent on the metal ions. Among them, Fe(III) ions afford the most significant fluorescence quenching effect. And almost no intensity change was observed in the case of other metal ions, suggesting that **1** and **4** have high selectivity for the detection of Fe(III) ions.

For the purpose of understanding the response of the fluorescence of **1** and **4** to the Fe(III) ion, the luminescence titration upon the addition of a solution of $Fe(NO_3)_3$ dissolved in DMF to **1** and **4** was further performed. Interestingly, the luminescence intensity of Fe(III)-incorporated **1** and **4** is dependent on the concentration of the Fe(III) ion. As shown in Fig. 12, nearly 100% of emission intensity was decreased monotonically and drastically when the Fe(III) ion concentration increased from 0 μL to 680 μL for **1** and 0 μL to 700 μL for **4**. To explore the luminescence quenching degree, the quenching coefficient was also calculated by using the Stern–Volmer equation: $I_0/I = 1 + K_{SV}[M]$ as mentioned above for acetone sensing. As shown

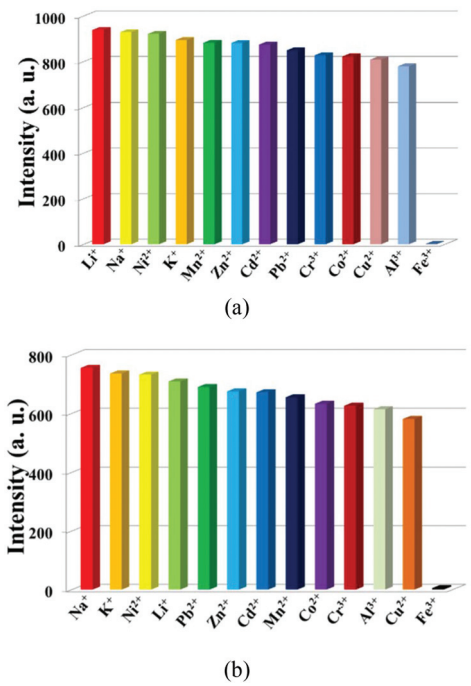

Fig. 11 (a) Photoluminescence intensities of **1** introduced into different metal ions dissolved in DMF when excited at 290 nm for **1**. (b) Photoluminescence intensities of **4** introduced into different metal ions dissolved in DMF when excited at 300 nm for **4**.

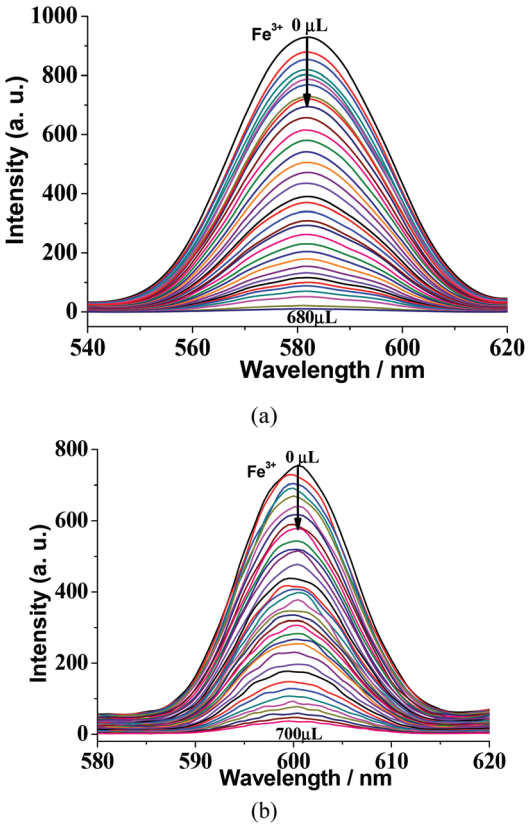

Fig. 12 (a) Photoluminescence spectra of the dispersed **1** in DMF in the presence of various contents of the Fe(III) ion (excited at 290 nm). (b) Photoluminescence spectra of the dispersed **4** in DMF in the presence of various contents of Fe(III) ion (excited at 300 nm).

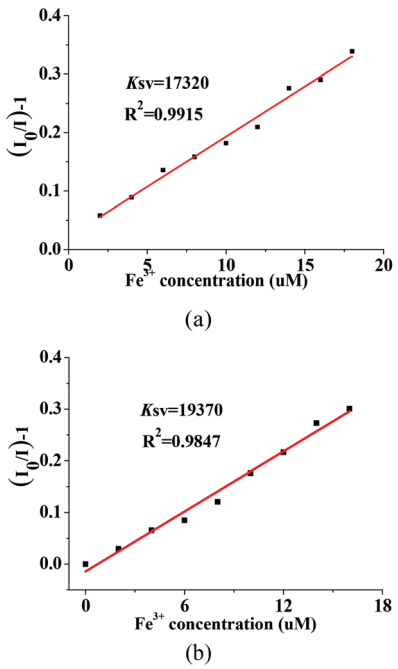

Fig. 13 (a) Stern–Volmer plot of **1** for the Fe(III) ion. (b) Stern–Volmer plot of **4** for the Fe(III) ion.

in Fig. 13, a good linear Stern–Volmer relationship is observed in **1** and **4** for Fe(III) ion sensing, suggesting that they are the dynamic quenching process for detecting Fe(III) ions. The K_{SV} values of **1** and **4** for sensing Fe(III) ions are 1.73 × 10^4 $M^{-1}$and 1.94 × 10^4 M^{-1}, respectively. Based on the K_{SV} values and the standard error (σ) for three repeated fluorescence measurements of blank solutions, the detection limits are estimated to be 152 ppb for **1** and 126 ppb for **4**. Comparing with reported MOFs, the K_{SV} values of **1** and **4** are relatively good under the same conditions.[37–41] Thus, **1** and **4** can be considered as potential candidates for selective sensing of the Fe(III) ion. Such fluorescence quenching is considered to be caused by the wide absorption between 250 and 500 nm of Fe(III), which is wider and stronger than other tested metal ions. The wide absorption of Fe(III) may hinder the absorption of **1** and **4** upon excitation, and lead to the decrease or quenching of the fluorescence.[42,43] As for the ketone molecule sensing, in addition to the energy transfer between the ligands and the ketone molecules as mentioned above, the competitive absorption of ketone molecules with organic ligands may also contribute to the fluorescence quenching since the tested ketone molecules have absorption in the range of 250–350 nm.[42]

Conclusions

In conclusion, in this work four new MOFs [Zn(L)(bpdc)]·1.6H_2O (**1**), [Co(L)(bpdc)]·H_2O (**2**), [Ni_3(L)$_2$(bptc)$_2$(H_2O)$_{10}$]·2H_2O (**3**) and [Cd_2(L)(Hbptc)$_2$] (**4**) were successfully synthesized by using mixed organic ligands. The high quenching efficiency and excellent selectivity of **1** and **4** for both ketone molecules and Fe(III) ions make them potential functional materials for the detection of ketone molecules and metal ions. In addition, compound **1** exhibits selective adsorption of CO_2 over N_2.

Conflicts of interest

There are no conflicts to declare.

Acknowledgements

We gratefully acknowledge the National Natural Science Foundation of China (grant no. 21331002 and 21573106) and the National Basic Research Program of China (grant no. 2017YFA0303500) for financial support of this work. The authors extend their appreciation to the International Scientific Partnership Program ISPP at King Saud University for funding this research work through ISPP#0090. This work was also supported by a Project Funded by the Priority Academic Program Development of Jiangsu Higher Education Institutions.

Notes and references

1 H. C. Zhou, J. R. Long and O. M. Yaghi, *Chem. Rev.*, 2012, **112**, 673.
2 H. X. Deng, C. J. Doonan, H. Furukawa, R. B. Ferreira, J. Towne, C. B. Knobler, B. Wang and O. M. Yaghi, *Science*, 2010, **327**, 846.
3 C. B. He, D. M. Liu and W. B. Lin, *Chem. Rev.*, 2015, **115**, 11079.
4 Y. B. Zhang, H. Furukawa, N. Ko, W. Nie, H. J. Park, S. Okajima, K. E. Cordova, H. Deng, J. Kim and O. M. Yaghi, *J. Am. Chem. Soc.*, 2015, **137**, 2641.
5 M. Kurmoo, *Chem. Soc. Rev.*, 2009, **38**, 1353.
6 J. R. Li, R. J. Kuppler and H. C. Zhou, *Chem. Soc. Rev.*, 2009, **38**, 1477.
7 H. L. Jiang and Q. Xu, *Chem. Commun.*, 2011, **47**, 3351.
8 Z. C. Hu, B. J. Deibert and J. Li, *Chem. Soc. Rev.*, 2014, **43**, 5815.
9 C. Zhang, Y. Che, Z. Zhang, X. Yang and L. Zang, *Chem. Commun.*, 2011, **47**, 2336.
10 H. Xu, J. K. Gao, X. F. Qian, J. P. Wang, H. J. He, Y. J. Cui, Y. Yang, Z. Y. Wang and G. D. Qian, *J. Mater. Chem. A*, 2016, **4**, 10900.
11 Y. Xiao, Y. Cui, Q. Zheng, S. Xiang, G. Qian and B. Chen, *Chem. Commun.*, 2010, **46**, 5503.
12 Z. Guo, H. Xu, S. Su, J. Cai, S. Dang, S. Xiang, G. Qian, H. Zhang, M. O'Keeffe and B. Chen, *Chem. Commun.*, 2011, **47**, 5551.
13 F. Y. Yi, W. Yang and Z. M. Sun, *J. Mater. Chem.*, 2012, **22**, 23201.
14 J. A. Hua, Y. Zhao, Y. S. Kang, Y. Lu and W. Y. Sun, *Dalton Trans.*, 2015, **44**, 11524.
15 Z. Q. Liu, Y. Zhao, Y. Deng, X. D. Zhang, Y. S. Kang, Q. Y. Lu and W. Y. Sun, *Sens. Actuators, B*, 2017, **250**, 179.
16 F. Y. Yi, J. P. Li, D. Wu and Z. M. Sun, *Chem. – Eur. J.*, 2015, **21**, 11475.
17 X. F. Zheng, L. Zhou, Y. M. Huang, C. G. Wang, J. G. Duan, L. L. Wen, Z. F. Tian and D. F. Li, *J. Mater. Chem. A*, 2014, **2**, 12413.
18 S. S. Chen, M. Chen, S. Takamizawa, M. S. Chen, Z. Su and W. Y. Sun, *Chem. Commun.*, 2011, **47**, 752.
19 S. S. Chen, M. Chen, S. Takamizawa, P. Wang, G. C. Lv and W. Y. Sun, *Chem. Commun.*, 2011, **47**, 4902.
20 R. T. Have, M. Huisman, A. Meetsma and A. M. Leusen, *Tetrahedron*, 1997, **53**, 11355.
21 *SAINT, Program for Data Extraction and Reduction*, Bruker AXS, Inc., Madison, WI, 2001.
22 G. M. Sheldrick, *SADABS, Program for Empirical Adsorption Correction of Area Detector Data*, University of Göttingen, Göttingen, Germany, 2003.
23 G. M. Sheldrick, *SHELXS-2014, Program for the Crystal Structure Solution*, University of Göttingen, Göttingen, Germany, 2014.
24 G. M. Sheldrick, *SHELXL-2014, Program for the Crystal Structure Solution*, University of Göttingen, Göttingen, Germany, 2014.
25 A. L. Spek, *Acta Crystallogr., Sect. A: Fundam. Crystallogr.*, 1990, **46**, 194.
26 A. L. Spek, *PLATON, A Multipurpose Crystallographic Tool*, Utrecht University, Utrecht, The Netherlands, 2005, or; A. L. Spek, *J. Appl. Crystallogr.*, 2003, **36**, 7.
27 V. A. Blatov, IUCr CompComm Newsletter, 2006, **7**, 4.
28 V. A. Blatov, *TOPOS, A multipurpose crystallochemical analysis with the program package topos*, Samara State University, Russia, 2009.
29 Z. Z. Xue, T. L. Sheng, Y. H. Wen, Y. Wang, M. Hu, R. B. Fu and X. T. Wu, *CrystEngComm*, 2015, **17**, 598.
30 C. Ma, C. Q. Jiao, Z. G. Sun, Y. Y. Zhu, X. W. Zhang, M. L. Wang, D. Yang, Z. Zhao, H. Y. Li and B. Xing, *RSC Adv.*, 2015, **5**, 79041.
31 Y. Deng, Z. Y. Yao, P. Wang, Y. Zhao, Y. S. Kang and W. Y. Sun, *Sens. Actuators, B*, 2017, **244**, 114.
32 G. Porter, S. K. Dogra, R. O. Loutfy, S. E. Sugrmori and R. W. Yip, *J. Chem. Soc., Faraday Trans. 1*, 1973, **69**, 1462.
33 H. Weng and B. Yan, *Sens. Actuators, B*, 2016, **228**, 702.
34 Y. Li, H. Song, Q. Chen, K. Liu, F. Y. Zhao, W. J. Ruan and Z. Chang, *J. Mater. Chem. A*, 2014, **2**, 9469.
35 F. Y. Yi, W. Yang and Z. M. Sun, *J. Mater. Chem.*, 2012, **22**, 23201.
36 H. N. Wang, S. Q. Jiang, Q. Y. Lu, Z. Y. Zhou, S. P. Zhuo, G. G. Shan and Z. M. Su, *RSC Adv.*, 2015, **5**, 48881.
37 B. Wang, Q. Yang, C. Guo, Y. X. Sun, L. H. Xie and J. R. Li, *ACS Appl. Mater. Interfaces*, 2017, **9**, 10286.
38 C. Zhang, Y. Yan, Q. Pan, L. Sun, H. He, Y. Liu, Z. Liang and J. Li, *Dalton Trans.*, 2015, **44**, 13340.
39 M. Zheng, H. Tan, Z. Xie, L. Zhang, X. Jing and Z. Sun, *ACS Appl. Mater. Interfaces*, 2013, **5**, 1078.
40 X. H. Zhou, L. Li, H. H. Li, A. Li, T. Yang and W. Huang, *Dalton Trans.*, 2013, **42**, 12403.
41 X. L. Zhao, D. Tian, Q. Gao, H. W. Sun, J. Xu and X. H. Bu, *Dalton Trans.*, 2016, **45**, 1040.
42 W. Yan, C. L. Zhuang, S. G. Chen, L. J. Han and H. G. Zheng, *ACS Appl. Mater. Interfaces*, 2017, **9**, 1629.
43 D. Zhan, X. H. Liu, Y. Zhao, P. Wang, Y. Liu, M. Azam, S. I. Al-Resayes, Y. Lu and W. Y. Sun, *J. Mater. Chem. A*, 2017, **5**, 15797.